Desalination and Water Treatment
www.deswater.com

doi: 10.5004/dwt.2021.27707

236 (2021) 171–181
October

Elucidation of the removal of trivalent and divalent heavy metal ions from aqueous solutions using hybrid-porous composite ion-exchangers by nonlinear regression

Sama M. Al-Jubouri[a,*], Sirhan I. Al-Batty[b], Rachel Ramsden[c], Julian Tay[d], Stuart M. Holmes[e]

[a]*Department of Chemical Engineering, College of Engineering, University of Baghdad, Aljadria, Baghdad, Postcode: 10071, Iraq, email: sama.al-jubouri@coeng.uobaghdad.edu.iq*
[b]*Department of Chemical & Process Engineering Technology, Jubail Industrial College, Kingdom of Saudi Arabia, email: batty_sa@jic.edu.sa*
[c]*BresMed Health Solutions Ltd., Sheffield S1 2GQ, UK, email: rramsden@bresmed.com*
[d]*ARLANXEO Singapore Pte Ltd., 3A International Business Park Rd, Singapore, email: juliantay1912@gmail.com*
[e]*Department of Chemical Engineering and Analytical Science, The University of Manchester, Manchester M13 9PL, UK, email: stuart.holmes@manchester.ac.uk*

Received 28 May 2021; Accepted 12 August 2021

ABSTRACT

The removal of trivalent and divalent heavy metal ions from aqueous solutions by the ion-exchange process was investigated via a theoretical study using two- and three-parameter isotherm models. Fe^{3+} and Ni^{2+} ions were chosen as models of trivalent and divalent heavy metal ions in this study. A hybrid zeolite/carbon composite was used to remove these ions from aqueous solutions in a batch test to provide the required data for the theoretical study. This work studied the effect of shaking time (0–24 h), pH solution (2–10), and initial ions concentration (50–500 ppm). The experimental data of ion-exchange of both metal ions were studied using the two-parameter isotherm models including Langmuir isotherm, Freundlich isotherm, and Temkin isotherm. Also, the experimental data of ion-exchange were studied using the three-parameter isotherm models including Hill isotherm, Khan isotherm, Redlich–Peterson isotherm, Radke–Prausnitz isotherm, Sips isotherm, Toth isotherm, Koble–Corrigan isotherm and Liu isotherm. The experimental data of ion-exchange of Fe^{3+} ions best fitted the Temkin isotherm. Also, they followed the three-parameter isotherm models comparably due to the correlation factor for all studied models ranging from 0.923–0.924 despite the values of some model parameters were away from reality. But, Koble–Corrigan isotherm was not applicable for Fe^{3+} ion-exchange. While the experimental data of ion-exchange of Ni^{2+} ions best fitted the Langmuir isotherm with $R^2 = 0.930$. Also, they fitted the three-parameter isotherm models indistinguishably despite some model parameters diverted away from reality. For both metal ions, the determined values of exponent of the Toth isotherm confirmed the system heterogeneity.

Keywords: Hybrid-porous composites; Zeolite; Heavy metals; Ion-exchange; Isotherm models

---

[*] Corresponding author.

1. Introduction

The overpopulation, industrial activities, and unplanned urbanization directly influence the continuous availability of freshwater over the world since it is an essential need for all living beings [1]. Water streams are accessible by various pollutants due to agricultural growth and rapid industrial activities [2] which makes the water pollution problem a global challenge [3]. The presence of metallic organic and inorganic species in the water bodies with concentrations that exceed the lethal dosage will harm the metabolic system [4]. Therefore, water bodies contaminated with poisonous heavy metal ions released from different industries are a threatening environment for aquatic beings' health and thus human health [5]. The presence of even low amounts of some heavy metals or radioactive elements such as zinc, manganese, nickel, lead, iron, copper, chromium, cadmium, arsenic, and cobalt, in natural water systems can enter into the human body causing malfunctions of many organs and therefore generate different problems such as vomiting, nervous system injuries, nausea, and bone difficulties [6–8]. For the last past decades, pollution by heavy metals pollution has become a serious concern because they can accumulate in the environment and are not biodegradable [9,10].

Heavy metals ions are discharged through the effluents of various industries such as metal processing, mining, battery industries, electroplating industries, tanneries industries, textile industries, pesticides industries, petroleum refining industries, pigment industries, paint industries, photographic industries, and printing industries [11]. As a consequence of the massive industrial wastewaters discharged annually, removal of pollutants especially heavy metals and radionuclides that result from nuclear activities is one of the most important matters [12]. Excessive accumulation of nickel ions in the human and biological bodies risks human life by causing function degradation of the lung, heart, kidney, and brain [13]. While, excessive inhalation of nickel causes chest pain, skin eruption, gastrointestinal ache, a dry cough, nausea, diarrhea, breathing problem, renal edema and pulmonary fibrosis [14]. Accordingly, the nickel concentration in drinking water should not exceed 0.07 ppm as stated by the World Health Organization [15]. Excessive iron endangers human health because of the toxicity of iron through the production of free radicals from a reaction between free ferrous iron and peroxides. These free radicals can damage DNA lipids, proteins and other cellular components because of their high reactivity. Also, the toxicity of iron causes problems of hypothermia, diarrhea, anorexia and cellular death therefore its concentration in drinking water should not exceed 0.3 ppm according to the World Health Organization. However, excessive level of iron in groundwater causes problems with plumbing fixtures, staining of laundry, turbidity, odor, metallic taste and growth of micro-organisms [16]. Therefore, and due to the consequences of these metals (whether trivalent or divalent), a frugal and effective removal process is necessary.

Different treatment methods have been mentioned in the literature such as solvent extraction, oxidation process, ion-exchange, adsorption, coagulation–precipitation, chemical precipitation evaporation, electrolysis and membrane technology including reverse osmosis, nanofiltration, microfiltration, ultrafiltration and electro-dialysis [17–19]. Numerous research papers have experienced adsorption and ion-exchange processes because the media chosen for such applications (such as zeolite in this work) are abundant, low-cost and have a large surface area. Therefore, these processes are feasible, cost-effective and effective [20,21]. Other research papers experienced adsorption by organic adsorbents such as citric anhydride anchored mesoporous metal organic framework (MOF) [22], heteroatom-doped magnetic hydrochar [23], and multi-walled carbon nanotubes [24,25], to remove different pollutants.

Zeolites are crystalline aluminosilicates minerals with open and accessible microporous framework structures made of SiO_4 tetrahedron and AlO_4 tetrahedron connected by sharing oxygen atoms [26]. Zeolites have been recognized as effective inexpensive adsorbents and ion-exchangers due to their open pores and channels which are filled by water that can be removed [27,28]. Zeolite structure contains positive cations that are balanced with the negative charge of zeolite structure and these non-structural cations are easy to exchange with the harmful cations. [29]. Hierarchically porous zeolite composites have been prepared in different ways and they proved their effectiveness in removing different heavy metals and radioactive elements because of the small amount of zeolites coating macroporous/mesoporous supports [30–32].

Unlike our previous work, this paper studies the behaviour of the zeolite/carbon composite in the removal of two different-charge heavy metals. Also, this work focuses on elucidating the zeolite/carbon composite behaviour through different isotherm models by non-linear regression. Two-parameter isotherm models such as Langmuir isotherm model, Freundlich isotherm model, Temkin isotherm model and Halsey isotherm model; and three-parameter isotherm models such as Hill isotherm model, Khan isotherm model, Redlich–Peterson isotherm model, Radke–Prausnitz isotherm model, Sips isotherm model, Toth isotherm model, Koble–Corrigan isotherm model and Liu isotherm model will be studied. A calculated correlation factor (R^2) will be used to judge the convergence between the experimental data and the isotherm models.

2. Experimental section

2.1. Methodology

The ion-exchanger used for this study was 4A zeolite/carbon composite that is prepared and characterized according to the procedures mentioned in previous work [32]. Briefly, 3.94 g of modified carbon was added to 48.71 g of a synthesis gel before crystallization at 100 C for 4 h. The characterization of this composite showed that it has a Si/Al ratio of 1, zeolite percentage of 41.98%wt. and BET surface area of 183.36 m^2/g. Similarly, ion-exchange experiments were carried out in the same way conducted in [32]. This was made by mixing a certain weight of ion-exchange material and 100 mL of a solution containing metal ions. The experiment time was set to 24 h to study the time effect and to figure out the equilibrium time for ion-exchange of 2 g zeolite composite for each liter of metal ions solution of 200 ppm. The experiment time for the other experiments studying the initial solution pH and initial metal ions concentration was set to 4 h. Both $NiSO_4·7H_2O$ (99.999%wt.) and $FeCl_3·6H_2O$ (97%wt.) were supplied by Sigma-Aldrich and used to prepare the metals ions solutions. The Ni^{2+} ions solutions showed a light turquoise color, while the Fe^{3+} ions solutions showed a bronze color.

NaOH (99.9%wt.) supplied by Fisher Scientific and hydrochloric acid (36%) supplied by BDH laboratory were used to adjust the pH of metal ions solutions during the treatment process. The effect of initial solution pH was studied at an ion-exchanger mass of 2 g/L of metal ions solution of 200 ppm. The initial pH values of the solutions of 200 ppm were measured to be 5.85 for the Ni^{2+} ions and 2.24 for Fe^{3+} ions. Also, the effect of initial metal ions concentration and the equilibrium isotherm models were studied at an ion-exchanger mass of 2 g/L of metal ions solution of 50, 100, 200, 300, 400 and 500 ppm. The samples were filtered, diluted and measured by Inductively Coupled Plasma-Optical Emission Spectroscopy (ICP-OES, model Vista-MPX by Varian) at a wavelength of 238.204 nm for iron and 231.6 nm of for nickel. The ion-exchange experiments and measurements were repeated three times to confirm the reliability of the obtained results. The repeated measurements were used to calculate the standard deviation.

3. Results and discussion

3.1. Ion-exchange

The results displaying the manner of NaA zeolite/carbon composite with divalent ion (Ni^{2+}) and trivalent ion (Fe^{3+}) are shown in Fig. 1. Starting with a 200 ppm Ni^{2+} ions initial concentration, the ion-exchange process took place and was kept for 24. The results of the remaining ions concentration against the contact time showed that the composites removed nearly 160 ppm Ni^{2+} ions, and 80 ppm Fe^{3+} ions at the same conditions; and the equilibrium likely occurred after 4 h of running the experiment. Perhaps the charge and the ionic radius of the exchanging ions which often affects the ion-exchange capacity and the overall selectivity order can explain the different affinity by the composite shown toward the two different-charge ions [14]. Typically, the selectivity increases with increasing the charge of the exchanging ions [33]; however, this would not eliminate the role of the ionic radius of the exchanging ions. Positively charged cations with small size can be surrounded by many shells of water molecules forming the hydration shell or hydrated radius. During ion-exchange, the cation with a hydration shell hardly enters zeolite pores impeding the occurrence of ion-exchange unless it is stripped [33]. The larger the ionic radius, the smaller the hydrated radius and higher affinity for ion-exchange [20]. The ionic radius of Ni^{2+} ion (0.72 Å [34]) is larger than the Fe^{3+} ion (0.6 Å (the larger hydrated radii)). Despite the higher charge of Fe^{3+} ions, the zeolite composite showed less affinity toward Fe^{3+} ions than Ni^{2+} ions which can be attributed to the large hydrated radius of Fe^{3+} ion (4.57 Å), comparing with Ni^{2+} ion (4.04 Å), which limits its access to the zeolite pores of 4 Å.

Fig. 2 shows the results presented as the remaining concentration of metal ions in solutions against the initial pH of the metal solutions. As the pH has a predominant role in the exchange process, it became necessary to compare its effect on the removal of two different-charge metals (such as trivalent and divalent). It was hard to raise the pH of Fe^{3+} ions solutions above 4 because it precipitated as $Fe(OH)_3$ in the form of bronze sludge. While no obstacle was encountered during increasing the initial pH from 2 to 10 for the Ni^{2+} ions solutions. Less concentration of Fe^{3+} ions remained in the solution at pH = 4, and the same behaviour was noticed when the pH of solutions containing Ni^{2+} ions was increased to 8 and 10. This is because acidic medium negatively influences zeolite structure by attacking the Al-linkage leading to

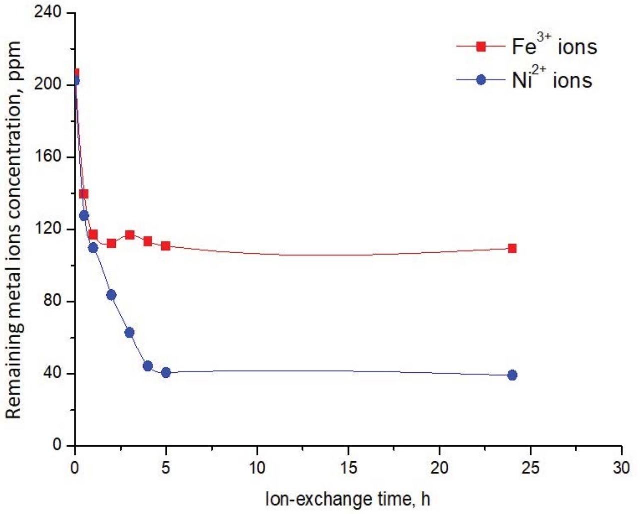

Fig. 1. The remaining concentration of the Fe^{3+} ions and Ni^{2+} ions after ion-exchange for 24 h, NaA zeolite/carbon per solution volume = 2 g/L, initial metal concentration = 200 ppm, mixing speed = 200 rpm, room temperature and normal solution pH. Standard deviation was 3.6% for Fe^{3+} ions and 1.8% for Ni^{2+} ions.

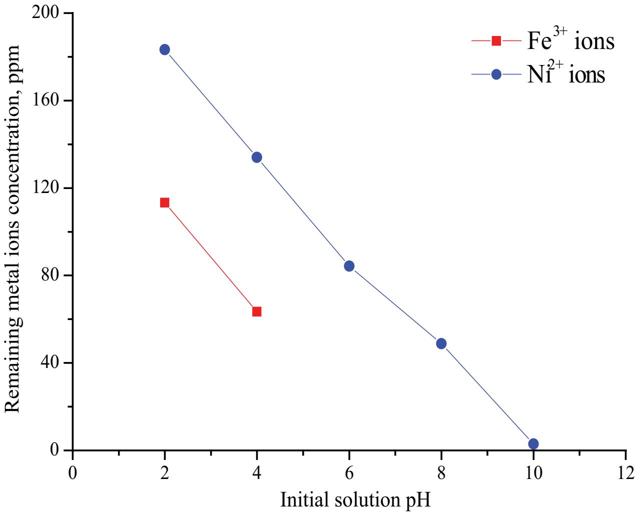

Fig. 2. The remaining concentration of the Fe^{3+} ions and Ni^{2+} ions after ion-exchange for 4 h, NaA zeolite/carbon per solution volume = 2 g/L, initial metal concentration = 200 ppm, mixing speed = 200 rpm, room temperature and different solution pH. Standard deviation was 2.8% for Fe^{3+} ions and 1.3% for Ni^{2+} ions.

dissociating it from zeolite structure. Besides, increasing the solution pH increases the competition among the metal ions and hydrogen ions for zeolite actives sites. Khana et al. [35] reported that less uptake of divalent metal cations occurred at low pH can perhaps be due to the competitive effect between the divalent metal cations and hydronium (H_3O^+) ions. Contrariwise, the high uptake of divalent metal cations that occurred at higher pH (just above 6) can be attributed to less concentration of the interfering H_3O^+ ions available in the aqueous medium.

Also, a comparison among the behaviour of Fe^{3+} ions and Ni^{2+} ions shows that the affinity of zeolite composites toward Ni^{2+} ions was less than toward Fe^{3+} ions. This can be explained by that the higher charge of Fe^{3+} ions allows it to win the competition against H^+ for zeolite actives sites.

The results explaining a comparison between Fe^{3+} ions and Ni^{2+} ions removed by zeolite/carbon composite at various initial ions concentrations are shown in Fig. 3. The results showed that a very massive difference between the remaining concentrations of Fe^{3+} ions and Ni^{2+} ions. Zeolite/carbon composite exhibited higher affinity toward Ni^{2+} ions than Fe^{3+} ions, therefore the remaining concentrations of Ni^{2+} ions were so lower than the remaining concentrations of Fe^{3+} ions at high initial metal concentrations especially between 300 and 500 ppm. This difference in the behaviour of zeolite composite can be attributed to the acidic nature of the Fe^{3+} ions that hinders the ion-exchange process. Besides, increasing the metal concentration increases the population of the competing Fe^{3+} ions for the same active sites number which in turn increases the exchange and thus the pH that causes precipitation of $Fe(OH)_3$.

All these experiments were conducted to obtain the experimental ion-exchange capacity values (q_e) for trivalent and divalent metals and use them together with the predicted equilibrium values ($q_{i\text{mod}}$) to investigate and find the best-fitting isotherm models, two/three-parameter models, via the correlation factor.

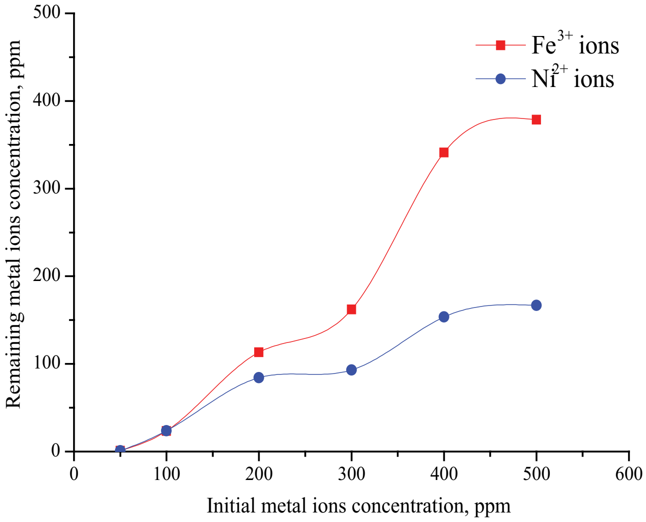

Fig. 3. The remaining concentration of the Fe^{3+} ions and Ni^{2+} ions after ion-exchange for 4 h, NaA zeolite/carbon per solution volume = 2 g/L, different initial metal concentration, mixing speed = 200 rpm, room temperature and normal solution pH. Standard deviation was 3.1% for Fe^{3+} ions and 2.7% for Ni^{2+} ions.

3.2. Equilibrium isotherms study

The results of studying the equilibrium isotherm models have been presented in the form of ion-exchange capacity q_e (mg metal ions/g media) that was determined using Eq. (1) verse equilibrium metal concentration C_e (ppm) [36].

$$q_e = \frac{\left(C_o - C_e\right)}{W_m} \times V_s \tag{1}$$

where C_o is the initial metal concentration (mg/L), W_m is the ion-exchanger mass (g) and V_s is the metal solution volume (L). R^2 was used to show the matching between the experimental results and the regression line of the isotherm model according to Eq. (2) [37].

$$R^2 = \left[\frac{\sum_1^n \left(q_{i_{\text{exp.}}} - q_{\text{av.exp.}}\right)^2 - \sum_1^n \left(q_{i_{\text{exp.}}} - q_{i.\text{mod.}}\right)^2}{\sum_1^n \left(q_{i_{\text{exp.}}} - q_{\text{av.exp.}}\right)^2}\right] \tag{2}$$

where n is the number of conducted experiments, $q_{i_{\text{exp.}}}$ is an experimental value of q_e, $q_{\text{av.exp.}}$ is the average of the experimental value of q_e and $q_{i_{\text{mod.}}}$ is a model value of q_e.

The mathematical equations that express the concentrations of a captured substance in a solid phase and its concentrations in a liquid phase at a constant pH and temperature are called adsorption isotherms [38]. These isotherms explain the mechanism by which a substance moves from an aqueous medium to a solid phase at equilibrium conditions. Therefore, numerous isotherm models have been established to depict the solid surface properties, the affinity of the solid materials and thus the uptake mechanism through determining the values of the model constants [39].

The nonlinear regression analysis has been adapted to calculate different isotherm parameters because the linearization of the isotherm equations causes the inseparable bias and changing the error structure of experimental data. Also, nonlinear regression analysis allows a mathematically precise calculating way of the models' parameters using the original form of isotherm equations [40]. Nonlinear regression incorporates minimizing the error between the experimental data points and the values theoretically predicted by a chosen isotherm model depending on its convergence standards [41]. In this study, solving the isotherm model equations was conducted by using the trial-and-error of the non-linear method via the solver add-in function in Microsoft excel.

3.2.1. Two-parameter isotherm models

Both the Langmuir isotherm model and the Freundlich isotherm model were used previously to model the experimental data of ion-exchange of heavy metals and radioactive elements by different zeolite composites [30,32,42,43].

Langmuir model presumes several assumptions such as maximum uptake capacity occurs when there is complete coverage of a monolayer of the adsorbate molecules on the adsorbent surface with no interactions between them. Also, it assumes each molecule is adsorbed at a specific site onto a homogeneous surface with equal energy and no transmigration occurs among the adsorbate molecules in the surface plane [39]. The non-linear form of the Langmuir model is given by Eq. (3) [37].

$$q_e = \frac{q_o \times b \times C_e}{1 + b \times C_e} \tag{3}$$

where q_e is the amount of metal ions removed at the equilibrium (according to Eq. (1), q_e is the ion-exchange capacity) (mg/g), C_e is the equilibrium metal ions concentration (mg/L), b is the Langmuir equilibrium constant (L/mg), and q_o is the maximum capacity of the ion-exchanger (mg/g) [44].

The Freundlich isotherm model is an empirical model that can be used for multilayer, reversible and non-ideal uptake over the heterogeneous surface plane with irregular distribution of affinities and heat of the uptake of the ions [45]. The Freundlich isotherm model can be expressed in Eq. (4) [46].

$$q_e = K_f \times C_e^{1/n} \tag{4}$$

where K_f is a constant of Freundlich isotherm that corresponds to uptake capacity (mg/g) and n is the intensity of uptake [47].

The Temkin isotherm model postulates increasing the surface coverage by the adsorbed molecules in a layer linearly reduces the heat of the adsorption of the molecules. The Temkin model takes into consideration the adsorbate-adsorbent interactions (heat of uptake). This model can be applied for the intermediate range of metal ions concentration and is not valid for extremely high and low concentrations [40]. The Temkin isotherm model can be represented by Eq. (5) [45].

$$q_e = \frac{R \times T}{b_T} \ln\left(A_T \times C_e\right) \tag{5}$$

where R is a gas constant (8.314 J/mol K), T is the absolute temperature (K), b_T is the Temkin isotherm constant ((J/mol)(g/mg)) which is the uptake energy difference and A_T is the equilibrium binding constant associated with the maximum energy of binding (L/mg) [48].

Halsey isotherm model suites to fit the experimental data of multilayer uptake that occurs at a relatively large distance from the surface and that happens by materials of heterogeneous nature [48]. The Halsey model can be represented by Eq. (6) [49].

$$q_e = \exp\left(\frac{\left(\ln K_H - \log C_e\right)}{n_H}\right) \tag{6}$$

where K_H is the constant of the Halsey model and n_H is the exponent of the Halsey model (dimensionless).

Fig. 4, Tables 1 and 2 present the results of fitting the equilibrium data to two-parameter isotherm models. The results show that the equilibrium data of Fe^{3+} ions fit the Temkin isotherm model confirmed by the higher value of R^2 more than other isotherm models. However, there is no significant difference in the values of the correlation factor of the Temkin isotherm model (R^2 = 0.922) and Langmuir isotherm model (R^2 = 0.920). This can be explained as the homogeneous coverage of the zeolite surface by Fe^{3+} ions within intermediate concentrations and all sites have equal energy. However, the results show that the equilibrium data of Ni^{2+} ions fit the Langmuir isotherm model with a higher value of an R^2 of 0.930 followed by the Freundlich isotherm model with an R^2 value of 0.893 then Temkin isotherm model with an R^2 value of 0.890. This result confirms occurring of homogenous coverage of the zeolite surface by Ni^{2+} ions with a possibility of the occurring multilayers uptake which caused higher uptake of Ni^{2+} ions as given by the ion-exchange results. A comparison between Fe^{3+} ions and Ni^{2+} ions based on the maximum uptake capacity determined using the Langmuir isotherm model show that the maximum capacity for Ni^{2+} ions approximately was four times this for Fe^{3+} ions. This can be attributed to that Ni^{2+}

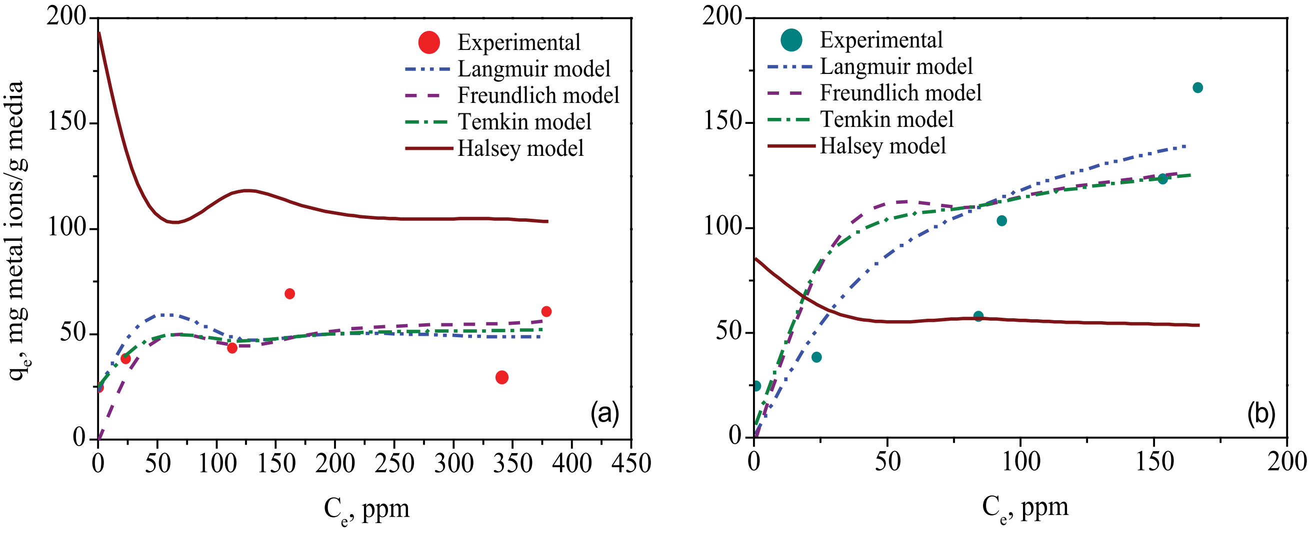

Fig. 4. Two-parameter uptake isotherms of (a) Fe^{3+} ions and (b) Ni^{2+} ions.

ions practiced multilayer ion-exchange and that was confirmed when making a comparison based on the K_f value obtained using the Freundlich isotherm model that corresponds to the ion-exchange capacity. Tables 1 and 2 show that the K_f value for Ni^{2+} ions was higher than the K_f value for Fe^{3+} ions.

For both metals ions, the Halsey isotherm model significantly deviated far from the equilibrium data with unacceptable values of R^2. This deviation can be attributed to that the uptake of ions did not occur on the layers far from the surface even though it occurred in multilayers.

3.2.2. Three parameter isotherm model

Hill isotherm model is used to describe the binding of various species onto homogeneous surfaces because it assumes that the uptake is a cooperative phenomenon. This is because the coordinate bonding at one site influences other binding sites on the same substrate surface [41]. This model can be given by Eq. (7) [37].

$$q_e = \frac{q_s \times C_e^n}{K_d + C_e^n} \tag{7}$$

where q_s is the maximum uptake capacity (mg/g), n is the exponent of the Hill model (dimensionless) and K_d is the constant of the Hill model $(mg/L)^n$.

The Khan isotherm model is suggested for the uptake from pure dilute aqueous solutions and it is expressed by Eq. (8) [50].

$$q_e = \frac{q_{\max} \times K_k \times C_e}{\left(1 + K_k \times C_e\right)^{n_k}} \tag{8}$$

where $q_{\max}$ is the theoretical isotherm saturation capacity (mg/g), n_k is the exponent of the Khan isotherm model (dimensionless) and K_k is a constant of the Khan isotherm model (L/mg).

Redlich-Peterson isotherm model gathers the parameters of the Langmuir and Freundlich isotherm models and can be applied for both heterogeneous and homogeneous sorption systems. The values of concentration in the numerator and an exponential function in the denominator define the Redlich–Peterson model to show the equilibrium of the uptake system [38]. The Redlich–Peterson isotherm model can be expressed by Eq. (9) [51].

Table 1
Model parameters of two-parameter isotherms for Fe^{3+} ions removal

Isotherm model	Model parameters		
Langmuir isotherm	q_o (mg/g)	b (L/mg)	R^2
model	48.869	1.073	0.920
Freundlich isotherm	K_f (mg/g)	n	R^2
model	30.563	3.233	0.862
Temkin isotherm model	b_T (J/mol)(g/mg)	A_T (L/mg)	R^2
	543.767	381.230	0.922
Halsey isotherm model	K_H	n_H	R^2
	2×10^{22}	9.788	0.031

Table 2
Model parameters of two-parameter isotherms for Ni^{2+} ions removal

Isotherm model	Model parameters		
Langmuir isotherm	q_o (mg/g)	b (L/mg)	R^2
model	195.420	0.016	0.930
Freundlich isotherm	K_f (mg/g)	n	R^2
model	70.868	2.851	0.893
Temkin isotherm	b_T (J/mol)(g/mg)	A_T (L/mg)	R^2
model	108.579	1.723	0.890
Halsey isotherm	K_H	n_H	R^2
model	3×10^{22}	11.713	0.6132

$$q_e = \frac{K_R \times C_e}{1 + a_s \times C_e^{B_s}} \tag{9}$$

where K_R and a_s are the constants of Redlich–Peterson isotherm model of (L/g) and $\left(\text{mg/L}\right)^{-B_s}$, respectively and B_s is the exponent of Redlich–Peterson model that should be ≤1 (dimensionless). This equation becomes linear at a low surface coverage ($B_s = 0$) and is reduced to the Langmuir isotherm when $B_s = 1$ [37]. At high concentration conditions, the Redlich–Peterson model approaches the Freundlich isotherm model, but it approaches the Langmuir isotherm model at low concentration [41].

Radke–Prausnitz isotherm model is similar to the Redlich–Peterson model and it has several preferable properties, therefore, it suites the uptake processes at low concentration as well as a wide range of adsorbate concentrations [40]. This model can be expressed by Eq. (10) [37].

$$q_e = \frac{q_{\max} \times K_{RP} \times C_e}{\left(1 + K_{RP} \times C_e\right)^{(1/n_{RP})}} \tag{10}$$

where $q_{\max}$ is the Radke–Prausnitz maximum uptake capacity (mg/g), K_{RP} is the equilibrium constant of Radke–Prausnitz model (L/mg), and n_{RP} is the exponent of Radke–Prausnitz model (dimensionless). Also, the Radke–Prausnitz model can be reduced to the Freundlich isotherm at high concentrations of adsorbate and to the Langmuir isotherm at $1/n_{RP}$ equals zero [37,40].

Sips isotherm model combines both Langmuir and Freundlich isotherms in an expression to predict the uptake in heterogeneous systems and avoid the limitation of using the Freundlich isotherm model at high adsorbate concentrations [41]. The Sips isotherm model can be expressed by Eq. (11) [37].

$$q_e = \frac{q_{\max} \times K_s \times C_e^{(1/n_s)}}{1 + K_s \times C_e^{(1/n_s)}} \tag{11}$$

where $q_{\max}$ is the maximum uptake capacity (mg/g), K_s is a constant of Sips isotherm model $\left(\text{L/mg}\right)^{1/n_s}$ and n_s is an exponent of the Sips isotherm model and $1/n_s$ should be

≤1 (dimensionless). The Sips isotherm is reduced to the Freundlich model at low adsorbate concentrations and to the Langmuir isotherm that gives the maximum capacity of the monolayer at high adsorbate concentrations [39]. Mainly, the equation parameters of the Sips isotherm model are dominated by temperature, pH and adsorbate concentration. Also, linearizing the model equation influences the values of the model isotherm constants [40].

Toth isotherm model is a useful improved modification of the Langmuir isotherm to describe heterogeneous uptake systems to satisfy both high and low-end boundaries of the concentrations [38]. The Toth isotherm model is expressed by Eq. (12) [37].

$$q_e = \frac{q_{\max} \times K_T \times C_e}{\left[1+\left(K_T \times C_e\right)^{(1/n_T)}\right]^{n_T}} \tag{12}$$

where $q_{\max}$ is the maximum uptake capacity (mg/g), K_T is a constant of Toth isotherm (L/mg) and n_T is the exponent of Toth isotherm (dimensionless). The constant n_T represents the heterogeneity of the uptake system; thus the system is heterogeneous when n_T deviated away from 1 [40]. At very low concentrations, the model equation can be reduced to Henry's law [45].

Koble–Corrigan isotherm model is a combination of both Langmuir and Freundlich isotherm models and is applied for heterogeneous uptake [38]. The Koble–Corrigan isotherm model is represented by Eq. (13) [52].

$$q_e = \frac{A \times C_e^n}{1+B \times C_e^n} \tag{13}$$

where A is the constant of Koble–Carrigan's isotherm ($L^n\ mg^{1-n}/g$), B is the constant of Koble–Carrigan's isotherm (L^n/mg^n) and n is the exponent of Koble–Carrigan's isotherm. The Koble–Corrigan isotherm model is reduced to the Freundlich isotherm at high adsorbate concentrations. This model is only applicable when the constant n is ≥1. Despite the high correlation coefficient or low error value, this model is incapable of describing the experimental data when $n < 1$ [40].

Liu isotherm model combines Langmuir and Freundlich isotherm models, but it discards several assumptions associated with both models. Since it discards the assumption of the monolayer of the Langmuir model and the assumption of infinite adsorption that initiates from the Freundlich model. The Liu model postulates that there is uniform energy in all active sites of the substrates. Unlike in the Freundlich isotherm model, the active sites should be saturated while the adsorbate molecules may prefer active sites presented by the adsorbent for occupation. The Liu isotherm model can be represented by Eq. (14) [37].

$$q_e = \frac{\left(q_{\max} \times K_g \times C_e\right)^{n_L}}{1+\left(K_g \times C_e\right)^{n_L}} \tag{14}$$

where K_g is the constant of Liu equilibrium (L/mg); n_L is the exponent of Liu model (dimensionless), and $q_{\max}$ is the maximum uptake capacity of the substrate (mg/g). The exponent n_L could be assumed any positive value unlike to Sips isotherm.

Figs. 5, 6, Tables 3 and 4 display the results of fitting the equilibrium data of the metals ions to three-parameter isotherm models. The results show that the equilibrium data of Fe^{3+} ion fitted to all three-parameter isotherm models with very close values of an R^2 (0.923–0.924). However, the equilibrium data of Ni^{2+} ion fitted the three-parameter isotherm models with the following order: Khan isotherm model = Liu isotherm model > Radke–Prausnitz isotherm model > Redlich–Peterson isotherm model > Hill isotherm model = Sips isotherm model > Koble–Corrigan isotherm model > Toth isotherm model.

The values of maximum uptake capacity displayed in Table 4 show that these values for Ni^{2+} ions were exaggeratedly higher than those for Fe^{3+} ions (see Table 3) except

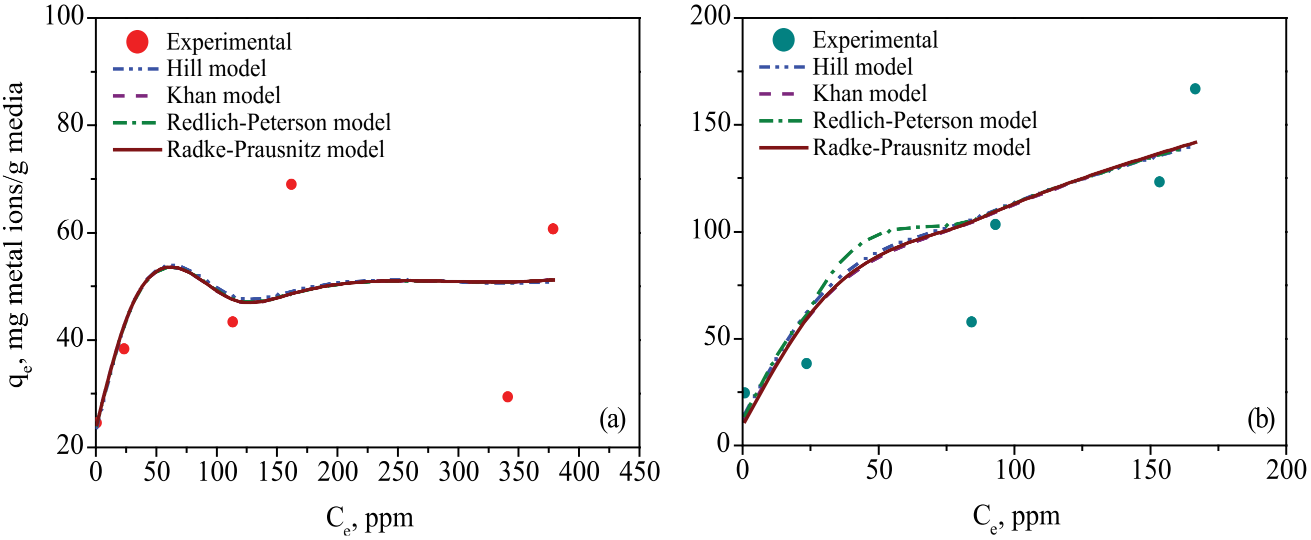

Fig. 5. Three-parameter uptake isotherms of (a) Fe^{3+} ions and (b) Ni^{2+} ions.

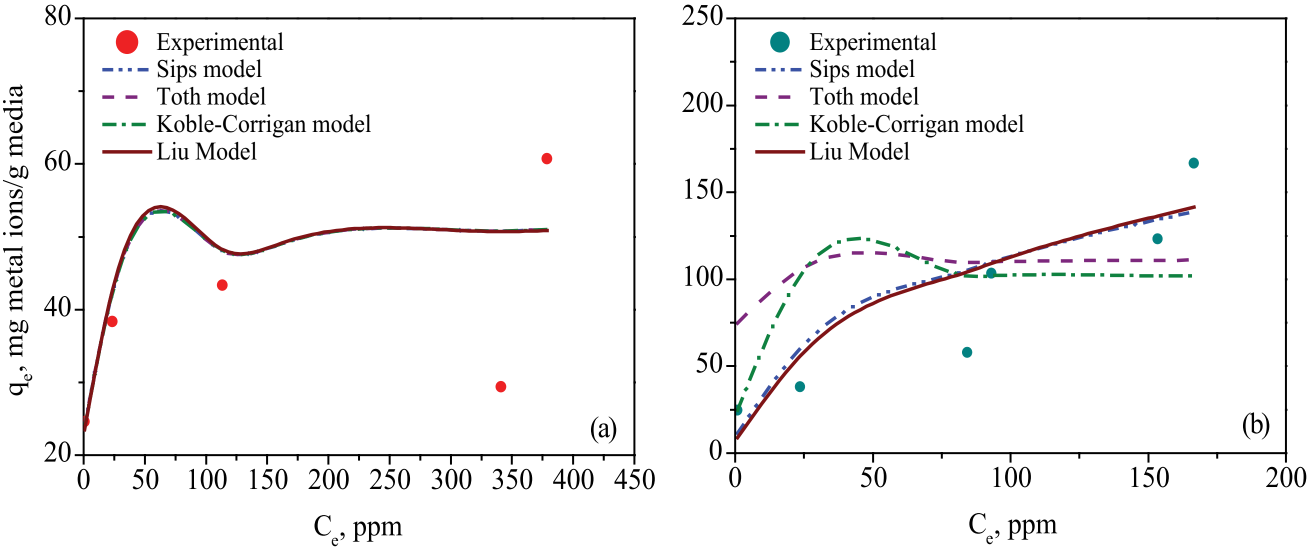

Fig. 6. Three-parameter uptake isotherms of (a) Fe^{3+} ions and (b) Ni^{2+} ions.

Table 3
Model parameters of three-parameter isotherms for Fe^{3+} ions removal

Isotherm model	Model parameters			
Hill isotherm model	q_s (mg/g)	n	K_d (mg/L)^n	R^2
	54.939	0.457	1.225	0.924
Khan isotherm model	$q_{\max}$ (mg/g)	K_k (L/mg)	n_k	R^2
	34.531	2.248	0.942	0.923
Redlich–Peterson isotherm model	K_R (L/g)	$a_s\left(\text{mg/L}\right)^{-B_s}$	B_s	R^2
	85.175	2.337	0.943	0.923
Radke–Prausnitz isotherm model	$q_{\max}$ (mg/g)	K_{RP} (L/mg)	n_{RP}	R^2
	35.539	2.247	1.062	0.923
Sips isotherm model	$q_{\max}$ (mg/g)	$K_s\left(\text{L/mg}\right)^{1/n_s}$	n_s	R^2
	55.781	0.796	2.287	0.924
Toth isotherm model	$q_{\max}$ (mg/g)	K_T (L/mg)	n_T	R^2
	57.133	19.052	2.791	0.924
Koble–Corrigan isotherm model	A (L^n mg^{1-n}/g)	n	B (L^n/mg^n)	R^2
	44.234	0.434	0.791	0.924
Liu isotherm model	$q_{\max}$ (mg/g)	K_g (L/mg)	n_L	R^2
	5,114.271	0.629	0.469	0.924

those for the Radke–Prausnitz isotherm model. For both ions, the determined values of B_s, which is the exponent of Redlich–Peterson, agreed to the condition of this model (should be ≤1), since they were 0.943 and 0.569 for Fe^{3+} ions and Ni^{2+} ions, respectively. Also, the determined values of n_s that is an exponent of the Sips isotherm model agreed to the condition of this model which is that $1/n_s$ should be ≤1. The values of n_s were 2.287 ($1/n_s = 0.437$) for Fe^{3+} ions and 1.962 ($1/n_s = 0.510$) for Ni^{2+} ions. The values of n_T representing the exponent of the Toth isotherm were 2.791 for Fe^{3+} ions and 1.980 for Ni^{2+} ions which are much higher than 1, thus the system is heterogeneous. The results presented in Table 4 show that the Koble–Corrigan isotherm model is only applicable for Ni^{2+} ions because n was 3.923 which is ≥1 but not applicable for Fe^{3+} ions even the high correlation coefficient ($R^2 = 0.924$) of this model (see Table 3). This can be attributed to the coverage of the ion-exchange heterogeneous surface with the trivalent Fe^{3+} ions being less than by divalent Ni^{2+} ions at the same conditions. Despite the exaggerated vales of $q_{\max}$ determined using the Liu model, the determined positive-values of n_L are in good agreement with the condition of this model.

4. Conclusions

In conclusion, the hybrid porous NaA zeolite/carbon composite showed a higher affinity toward Ni^{2+} ions than Fe^{3+} ions which can be attributed to the smaller ionic radius

Table 4
Model parameters of three-parameter isotherms for Ni^{2+} ions removal

Isotherm model	Model parameters			
Hill isotherm model	q_s (mg/g)	n	K_d $(mg/L)^n$	R^2
	502,788.800	0.417	30,148.49	0.938
Khan isotherm model	$q_{\max}$ (mg/g)	K_k (L/mg)	n_k	R^2
	2.639	43.934	0.552	0.942
Redlich–Peterson isotherm model	K_R (L/g)	$a_s\left(\text{mg/L}\right)^{-B_s}$	B_s	R^2
	14,115.070	907.659	0.569	0.940
Radke–Prausnitz isotherm model	$q_{\max}$ (mg/g)	K_{RP} (L/mg)	n_{RP}	R^2
	7.991	3.964	1.796	0.941
Sips isotherm model	$q_{\max}$ (mg/g)	$K_s\left(\text{L/mg}\right)^{1/n_s}$	n_s	R^2
	602.256	0.022	1.962	0.938
Toth isotherm model	$q_{\max}$ (mg/g)	K_T (L/mg)	n_T	R^2
	114.604	21.888	1.980	0.791
Koble–Corrigan isotherm model	A (L^n mg^{1-n}/g)	n	B (L^n/mg^n)	R^2
	91.258	3.923	0.895	0.829
Liu isotherm model	$q_{\max}$ (mg/g)	K_g (L/mg)	n_L	R^2
	105,591.400	0.000651	0.557	0.942

that Fe^{3+} ions have despite its higher charge. The opposite was obtained when performing the ion-exchange at different pH solutions however there was no chance to raise the pH of the Fe^{3+} ions solution above 4 due to the Fe^{3+} ions precipitation. The results of nonlinear regression revealed that the ion-exchange experimental data of Fe^{3+} and Ni^{2+} ions removed by the hybrid-porous composite fitted the studied models differently. The correlation factor values were used to determine the best fit of the ion-exchange experimental data to the two- and three-parameter isotherm models. The experimental data of Fe^{3+} ion-exchange were best described by Temkin isotherm followed by the Langmuir isotherm and the Freundlich isotherm. While the experimental data of Ni^{2+} ion-exchange were best represented by the Langmuir isotherm followed by the Freundlich isotherm and the Temkin isotherm. The three-parameter isotherm models fitted to the ion-exchange experimental data of Fe^{3+} ions in a like manner and correlation factor values ranged from 0.923 to 0.924. For some models, the values of the determined model parameters were away from reality and the Koble–Corrigan isotherm model was not applicable for Fe^{3+} ions. The experimental data of Ni^{2+} ion-exchange are best described by the three-parameter isotherm models except for the Koble–Corrigan isotherm and Toth isotherm which have fewer R^2 values. Some of the determined model parameters of Ni^{2+} ion-exchange were significantly far from what they should be in fact. Since the calculated value of the exponent of the Toth isotherm was much higher than 1, the system is heterogeneous.

Declarations

Conflicts of interest/Competing interests: The authors declare that they have no known competing financial interests or personal relationships that could have appeared to influence the work reported in this paper.

Availability of data and material (data transparency): The authors confirm the availability of data and material.

References

[1] U.P. Kiruba, P.S. Kumar, C. Prabhakaran, V. Aditya, Characteristics of thermodynamic, isotherm, kinetic, mechanism and design equations for the analysis of adsorption in Cd(II) ions-surface modified Eucalyptus seeds system, J. Taiwan Inst. Chem. Eng., 45 (2014) 2957–2968.

[2] Z. Hajahmadi, H. Younesi, N. Bahramifar, H. Khakpour, K. Pirzadeh, Multicomponent isotherm for biosorption of Zn(II), Co(II) and Cd(II) from ternary mixture onto pretreated dried *Aspergillus niger* biomass, Water Resour. Ind., 11 (2015) 71–80.

[3] U. Maheshwari, B. Mathesan, S. Gupta, Efficient adsorbent for simultaneous removal of Cu(II), Zn(II) and Cr(VI): kinetic, thermodynamics and mass transfer mechanism, Process Saf. Environ. Prot., 98 (2015) 198–210.

[4] M. Kapur, M.K. Mondal, Competitive sorption of Cu(II) and Ni(II) ions from aqueous solutions: kinetics, thermodynamics and desorption studies, J. Taiwan Inst. Chem. Eng., 45 (2014) 1803–1813.

[5] B. Singha, S.K. Das, Adsorptive removal of Cu(II) from aqueous solution and industrial effluent using natural/agricultural wastes, Colloids Surf., B, 107 (2013) 97–106.

[6] Z.A. Alothman, A review: fundamental aspects of silicate mesoporous materials, Materials, 5 (2012) 2874–2902.

[7] Z.A. Alothman, A.H. Bahkali, M.A. Khiyami, S.M. Alfadul, S.M. Wabaidur, M. Alam, B.Z. Alfarhan, Low cost biosorbents from fungi for heavy metals removal from wastewater, Sep. Sci. Technol., 55 (2020) 1766–1775.

[8] A. Mittal, M. Naushad, G. Sharma, Z.A. Alothman, S.M. Wabaidur, M. Alam, Fabrication of MWCNTs/ThO_2 nanocomposite and its adsorption behavior for the removal of Pb(II) metal from aqueous medium, Desal. Water Treat., 57 (2015) 21863–21869.

[9] P. SenthilKumar, S. Ramalingam, V. Sathyaselvabala, S.D. Kirupha, S. Sivanesan, Removal of copper(II) ions from aqueous solution by adsorption using cashew nut shell, Desalination, 266 (2011) 63–71.

[10] R.T. Hadi, A.B. Salman, S. Nabeel, S.A. Soud, Recovery of lead from simulated wastewater by using stainless steel rotating

cylinder electrode electrochemical reactor, Desal. Water Treat., 99 (2017) 266–271.

[11] M. Ahmaruzzaman, Industrial wastes as low-cost potential adsorbents for the treatment of wastewater laden with heavy metals, Adv. Colloid Interface Sci., 166 (2011) 36–59.

[12] D. Ding, Y. Zhao, S. Yang, W. Shi, Z. Zhang, Z. Lei, Y. Yang, Adsorption of cesium from aqueous solution using agricultural residue-walnut shell: equilibrium, kinetic and thermodynamic modeling studies, Water Res., 47 (2013) 2563–2571.

[13] W.X. Zhou, D.G. Guan, Y. Sun, C.M. Sun, G.L. Xu, T. Chen, Z.S. Yu, Y. Xu, H. Yan, Removal of nickel(II) Ion from wastewater by modified maifanite, Mater. Sci. Forum, 814 (2015) 371–375.

[14] Inamuddin, M.I. Ahamed, A.M. Asiri, Applications of Ion Exchange Materials in the Environment, Springer International Publishing, Cham, 2019.

[15] S.M. Al-Jubouri, H.A. Sabbar, H.A. Lafta, B.I. Waisi, Effect of synthesis parameters on the formation 4A zeolite crystals: characterization analysis and heavy metals uptake performance study for water treatment, Desal. Water Treat., 165 (2019) 290–300.

[16] M.M.H. Khalil, K.Z. Al-Wakeel, S.S. Abd El Rehim, H. Abd El Monem, Efficient removal of ferric ions from aqueous medium by amine modified chitosan resins, J. Environ. Chem. Eng., 1 (2013) 566–573.

[17] J.C. Igwe, A.A. Abia, Adsorption isotherm studies of Cd(II), Pb(II) and Zn(II) ions bioremediation from aqueous solution using unmodified and EDTA-modified maize cob, Eclética Química, 32 (2007) 33–42.

[18] H. Wang, X. Yuan, Y. Wu, H. Huang, G. Zeng, Y. Liu, X. Wang, N. Lin, Y. Qi, Adsorption characteristics and behaviors of graphene oxide for Zn(II) removal from aqueous solution, Appl. Surf. Sci., 279 (2013) 432–440.

[19] M. del R.M. Virgen, O.F.G. Vázquez, V.H. Montoya, R.T. Gómez, Removal of Heavy Metals Using Adsorption Processes Subject to an External Magnetic Field, H. El-Din M. Saleh, R.F. Aglan, Eds., Heavy Metals, 2018, p. 253, doi: 10.5772/intechopen.74050.

[20] X. Zhang, Y. Hao, X. Wang, Z. Chen, C. Li, Competitive adsorption of cadmium(II) and mercury(II) ions from aqueous solutions by activated carbon from *Xanthoceras sorbifolia* bunge hull, J. Chem., 2016 (2016), doi: 10.1155/2016/4326351.

[21] M.N. Carvalho, C.A. De Abreu, M. Benachour, D.C. Sales, O.S. Baraúna, M.A. Da Motta Sobrinho, Applying combined Langmuir–Freundlich model to the multi-component adsorption of BTEX and phenol on smectite clay, Adsorpt. Sci. Technol., 30 (2012) 691–700.

[22] A.A. Alqadami, M.A. Khan, M.R. Siddiqui, Z.A. Alothman, Development of citric anhydride anchored mesoporous MOF through post synthesis modification to sequester potentially toxic lead(II) from water, Microporous Mesoporous Mater., 261 (2018) 198–206.

[23] M.A. Khan, A.A. Alqadami, M. Otero, M.R. Siddiqui, Z.A. Alothman, I. Alsohaimi, M. Rafatullah, A.E. Hamedelniel, Heteroatom-doped magnetic hydrochar to remove post-transition and transition metals from water: synthesis, characterization, and adsorption studies, Chemosphere, 218 (2019) 1089–1099.

[24] I. Ali, O.M. Alharbi, Z.A. ALOthman, A.M. Al-Mohaimeed, A. Alwarthan, Modeling of fenuron pesticide adsorption on CNTs for mechanistic insight and removal in water, Environ. Res., 170 (2019) 389–397.

[25] Z.A. ALOthman, A.Y. Badjah, I. Ali, Facile synthesis and characterization of multi walled carbon nanotubes for fast and effective removal of 4-tert-octylphenol endocrine disruptor in water, J. Mol. Liq., 275 (2019) 41–48.

[26] S.M. Al-Jubouri, B.I. Waisi, S.M. Holmes, Rietveld texture refinement analysis of Linde type A zeolite from X-ray diffraction data, J. Eng. Sci. Technol., 13 (2018) 4066–4077.

[27] S.M. Al-Jubouri, The static aging effect on the seedless synthesis of different ranges Faujasite-type zeolite Y at various factors, Iraqi J. Chem. Pet. Eng., 20 (2019) 7–13.

[28] S.M. Al-Jubouri, S.I. Al-Batty, S.M. Holmes, Using the ash of common water reeds as a silica source for producing high purity ZSM-5 zeolite microspheres, Microporous Mesoporous Mater., 316 (2021) 110953, doi: 10.1016/j.micromeso.2021.110953.

[29] S.M. Al-Jubouri, Synthesis of hierarchically porous ZSM-5 zeolite by self-assembly induced by aging in the absence of seeding-assistance, Microporous Mesoporous Mater., 303 (2020) 110296, doi: 10.1016/j.micromeso.2020.110296.

[30] D.A. De Haro-Del Rio, S.M. Al-Jubouri, S.M. Holmes, Hierarchical porous structured zeolite composite for removal of ionic contaminants from waste streams, Chim. Oggi – Chem. Today, 35 (2017) 26–29.

[31] S.M. Al-Jubouri, D.A. De Haro-Del Rio, A. Alfutimie, N.A. Curry, S.M. Holmes, Understanding the seeding mechanism of hierarchically porous zeolite/carbon composites, Microporous Mesoporous Mater., 268 (2018) 109–116.

[32] S.M. Al-Jubouri, S.M. Holmes, Immobilization of cobalt ions using hierarchically porous 4A zeolite-based carbon composites: ion-exchange and solidification, J. Water Process Eng., 33 (2020) 101059, doi: 10.1016/j.jwpe.2019.101059.

[33] M. Luqman, Ion Exchange Technology I: Theory and Materials (Vol. 1), Springer Science & Business Media, 2012.

[34] I. Mobasherpour, E. Salahi, M. Pazouki, Comparative of the removal of Pb^{2+}, Cd^{2+} and Ni^{2+} by nano crystallite hydroxyapatite from aqueous solutions: adsorption isotherm study, Arabian J. Chem., 5 (2012) 439–446.

[35] M.A. Khan, A.A. Alqadami, S.M. Wabaidur, M.R. Siddiqui, B.-H. Jeon, S.A. Alshareef, Z.A. Alothman, A.E. Hamedelniel, Oil industry waste based non-magnetic and magnetic hydrochar to sequester potentially toxic post-transition metal ions from water, J. Hazard. Mater., 400 (2020) 123247, doi: 10.1016/j.jhazmat.2020.123247.

[36] A.S. Yaro, M.H. Al-Hassani, H.A.K. Rasheed, Treatment copper biosorption using local Iraqi natural agents, Desal. Water Treat., 54 (2015) 533–539.

[37] É.C. Lima, M.A. Adebayo, F.M. Machado, Kinetic and Equilibrium Models of Adsorption, C.P. Bergmann, F.M. Machado, Eds., Carbon Nanomaterials as Adsorbents for Environmental and Biological Applications, Springer, Cham, 2015, pp. 33–69.

[38] M.A. Hossain, H.H. Ngo, W.S. Guo, T. V. Nguyen, Palm oil fruit shells as biosorbent for copper removal from water and wastewater: experiments and sorption models, Bioresour. Technol., 113 (2012) 97–101.

[39] A.M. Vargas, A.L. Cazetta, M.H. Kunita, T.L. Silva, V.C. Almeida, Adsorption of methylene blue on activated carbon produced from flamboyant pods (Delonix regia): study of adsorption isotherms and kinetic models, Chem. Eng. J., 168 (2011) 722–730.

[40] N. Ayawei, A.N. Ebelegi, D. Wankasi, Modelling and interpretation of adsorption isotherms, J. Chem., 2017 (2017), doi: 10.1155/2017/3039817.

[41] K.Y. Foo, B.H. Hameed, Insights into the modeling of adsorption isotherm systems, Chem. Eng. J., 156 (2010) 2–10.

[42] S.M. Al-Jubouri, N.A. Curry, S.M. Holmes, Hierarchical porous structured zeolite composite for removal of ionic contaminants from waste streams and effective encapsulation of hazardous waste, J. Hazard. Mater., 320 (2016) 241–251.

[43] S.M. Al-Jubouri, S.M. Holmes, Hierarchically porous zeolite X composites for manganese ion-exchange and solidification: equilibrium isotherms, kinetic and thermodynamic studies, Chem. Eng. J., 308 (2017) 476–491.

[44] Q. Ge, M. Moeen, Q. Tian, J. Xu, K. Feng, Highly effective removal of Pb^{2+} in aqueous solution by Na-X zeolite derived from coal gangue, Environ. Sci. Pollut. Res., 27 (2020) 7398–7408.

[45] S.A. Ghorbanian, N. Bagheri, A. Khakpay, Investigation of Adsorption Isotherms of Benzoic Acid on Activated Carbon, 1st National Conference on Industrial Water and Wastewater Treatment, Mahshahr, Iran, 2012, pp. 1–5.

[46] T.P. Belova, Adsorption of heavy metal ions (Cu^{2+}, Ni^{2+}, Co^{2+} and Fe^{2+}) from aqueous solutions by natural zeolite, Heliyon, 5 (2019) e02320, doi: 10.1016/j.heliyon.2019.e02320.

[47] A. Maleki, M. Mohammad, Z. Emdadi, N. Asim, M. Azizi, J. Safaei, Adsorbent materials based on a geopolymer paste for dye removal from aqueous solutions, Arabian J. Chem., 13 (2020) 3017–3025.

[48] M.R. Samarghandi, M. Hadi, S. Moayedi, F.B. Askari, Two-parameter isotherms of methyl orange sorption by pinecone derived activated carbon, Iran. J. Environ. Health Sci. Eng., 6 (2009) 285–294.

[49] M.T. Amin, A.A. Alazba, M. Shafiq, Adsorptive removal of reactive black 5 from wastewater using bentonite clay: isotherms, kinetics and thermodynamics, Sustainability, 7 (2015) 15302–15318.

[50] A. Abdolali, H.H. Ngo, W. Guo, S. Lu, S.S. Chen, N.C. Nguyen, X. Zhang, J. Wang, Y. Wu, A breakthrough biosorbent in removing heavy metals: equilibrium, kinetic, thermodynamic and mechanism analyses in a lab-scale study, Sci. Total Environ., 542 (2016) 603–611.

[51] A.H. Ali, Comparative study on removal of cadmium(II) from simulated wastewater by adsorption onto GAC, DB, and PR, Desal. Water Treat., 51 (2013) 5547–5558.

[52] M. Zhang, H. Zhang, D. Xu, L. Han, D. Niu, B. Tian, J. Zhang, L. Zhang, W. Wu, Removal of ammonium from aqueous solutions using zeolite synthesized from fly ash by a fusion method, Desalination, 271 (2011) 111–121.